Probing degrees of orientation of polar molecules with harmonic emission in ultrashort laser pulses

Y. Z. Shi,[1] B. Zhang,[2] W. Y. Li,[3,4,*] S. J. Yu,[1] and Y. J. Chen[1,†]

[1]*College of Physics and Information Technology, Shaan'xi Normal University, Xi'an 710119, China*

[2]*Department of Physics, Harbin Institute of Technology, Harbin 150001, China*

[3]*College of Physics and Information Engineering, Hebei Normal University, Shijiazhuang 050024, China*

[4]*School of Mathematics and Science, Hebei GEO University, Shijiazhuang 050031, China*

(Received 13 December 2016; revised manuscript received 7 February 2017; published 8 March 2017)

The orientation of molecules with respect to the laser polarization brings rich physics into laser-molecule interaction. However, the degree of orientation of a polar molecule is difficult to measure in present experiments. Here, through numerical solution of the time-dependent Schrödinger equation, we show that high-order-harmonic generation from polar molecules with a large permanent dipole in ultrashort laser pulses can be used as a sensitive tool to probe the degree of orientation. The underlying mechanism is discussed.

DOI: 10.1103/PhysRevA.95.033406

I. INTRODUCTION

The alignment of molecules in a gas phase by means of laser fields has wide applications in photochemistry [1] and attosecond physics [2]. For example, with aligned molecules, the measurement of the high-order-harmonic generation (HHG) signal allows one to reconstruct the highest occupied molecular orbital (HOMO) [3], probe multielectron dynamics [4], and follow a chemical reaction [5]. For asymmetric molecules, besides the alignment, the orientation of the sample where the molecules are arranged in a "head-versus-tail" order [6–10] is also especially important in ultrafast measurements such as asymmetric orbital imaging [11–14] and attosecond probing of the electron dynamics under the influence of the asymmetric potential [15–19] with odd-even HHG. In real experiments, however, perfect orientation is impossible and the degree of orientation cannot be directly measured [20]. As many theoretical and experimental procedures in ultrafast measurements of asymmetric systems are closely associated with the degree of orientation [12,17], to evaluate the degree of orientation achieved in experiments is the first step to understand the relevant experimental results.

On the other hand, with the development of laser technology, strong ultrashort laser pulses with only a few optical cycles (o.c.) [21–23] have become available in recent years, which have important applications in attosecond science [24,25]. Since the carrier-envelope phase (CEP) effectively determines the peak position of the electric field in an ultrashort pulse, the strong-field-induced processes such as above-threshold ionization and HHG [26] are sensitive to CEP [27–30]. However, for atoms and symmetric molecules interacting with linearly polarized laser fields, the HHG power spectrum as well as the ionization yields are invariant when the CEP changes by π because of the inversion symmetry in such systems. In contrast, due to the existence of the permanent dipole [31–33], the ionization and harmonic emission from asymmetric molecules such as HeH^{2+} [34–36] differ remarkably when the CEP has a π-phase jump. It has been shown that as the laser polarization is parallel (antiparallel) to the permanent dipole the ground-state energy of the asymmetric molecule HeH^{2+} is dressed down (up), resulting in the asymmetric ionization of the system in one optical cycle [37]. This asymmetric ionization along with the effect of Coulomb focusing also leads to the asymmetry in harmonic emission from the system [38].

In this paper, we study the HHG from asymmetric molecules in ultrashort laser pulses through numerical solution of the time-dependent Schrödinger equation (TDSE). For two CEPs of ϕ_0 and $\phi_0+\pi$ with a π phase difference, these two calculated HHG spectra differ importantly from each other in the high-energy region. This phenomenon holds as we change the value of ϕ_0 which is not easy to manipulate in experiments. We show that the phenomenon is closely associated with the effect of the permanent dipole and is also very sensitive to the degree of orientation of the asymmetric system. A simple model which considers imperfect orientation is developed to describe the HHG of an asymmetric molecule with a large permanent dipole in ultrashort laser pulses. With this model, we show that the HHG spectrum in the high-energy region in ultrashort pulses can be used as a tool to calibrate the degree of orientation.

II. NUMERICAL METHODS

We begin our discussions for the simple asymmetric molecule HeH^{2+} with 1σ symmetry. Then we extend our considerations to asymmetric molecules with more complex symmetries such BF and CO with 5σ symmetry.

The Hamiltonian of the asymmetric system studied here has the following form of $H(t)=\mathbf{p}^2/2+V(\mathbf{r})+\mathbf{r}\cdot\mathbf{E}(t)$ (in atomic units of $\hbar=e=m_e=1$). For HeH^{2+}, we use the soft-Coulomb potential of $V(\mathbf{r})=-Z_1/\sqrt{\xi+(x+R_1\cos\theta)^2+(y+R_1\sin\theta)^2}-Z_2/\sqrt{\xi+(x-R_2\cos\theta)^2+(y-R_2\sin\theta)^2}$ in two-dimensional cases. Here $Z_2=1.62$ and $Z_1=Z_2/2$ are the effective charges of the He and H cores, respectively. $R_1=Z_2R/(Z_1+Z_2)$, $R_2=Z_1R/(Z_1+Z_2)$, and $R=4$ a.u. is the internuclear distance. $\xi=0.05$ is the smoothing parameter which is used to avoid the Coulomb singularity. The energy of the 1σ ground state and the 2σ first excited state reproduced here, through the imaginary-time

*liweiyanhb@126.com

†chenyanjun@snnu.edu.cn

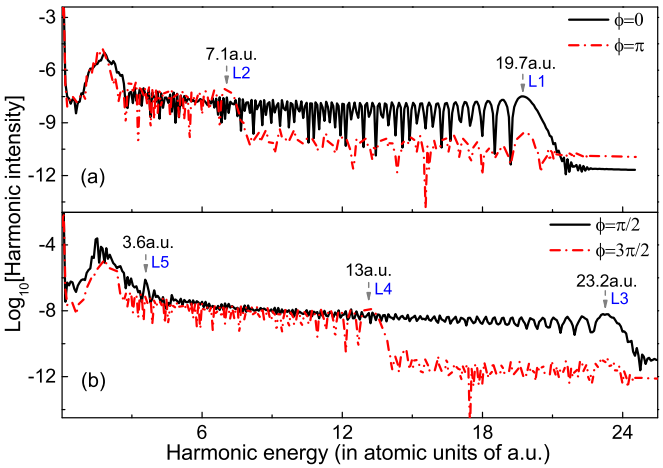

FIG. 1. HHG power spectra of HeH^{2+} exposed to a three-cycle laser pulse for different CEPs of (a) $\phi = 0$ and π and (b) $\phi = \pi/2$ and $3\pi/2$ at $\theta = 0^\circ$. The laser wavelength used here is $\lambda = 600$ nm and the peak intensity is $I = 5 \times 10^{15}$ W/cm^2. The cutoffs in the spectra are indicated by the vertical arrows. The black numbers denote the corresponding energy of the cutoffs. The blue symbols denote the corresponding trajectories of the cutoffs introduced in Fig. 2.

propagation method, is $E_0 = -2.25$ a.u. and $E_1 = -1.12$ a.u., respectively. These values are near to the real ones of HeH^{2+} (i.e., $E_0 = -2.25$ a.u. and $E_1 = -1.03$ a.u., calculated using the approach introduced in [37]). θ is the angle between the molecular axis and the laser polarization. The permanent dipole of the asymmetric molecule directing from the He nucleus to the H nucleus is antiparallel to the x axis here.

The laser field $\mathbf{E}(t)$ used here has the form of $\mathbf{E}(t) = \vec{\mathbf{e}} f(t)\varepsilon_0 \sin(\omega_0 t + \phi)$. Here, ε_0 is the laser amplitude, ω_0 is the laser frequency, $f(t)$ is the envelope function, and ϕ is the CEP. $\vec{\mathbf{e}}$ is the unit vector along the laser polarization which is along the x axis here.

In our calculations, we use a three-cycle sin-square-envelope pulse. The TDSE of $i\dot{\psi}(t) = H(t)\psi(t)$ is solved numerically by the spectral method [39], with 2048 time steps in each laser cycle. We work with a space grid size of $L_x \times L_y = 1638.4 \times 102.4$ a.u. for the x and y axes. The space step is $\Delta x = \Delta y = 0.4$ a.u.. In each time step, a mask function $\cos^{1/8}$ is used in the boundary to absorb the continuum wave packet. The coherent part of the harmonic spectra parallel to the laser polarization can be evaluated using [40] $F(\omega) = \int \langle \psi(t)|\vec{\mathbf{e}} \cdot \nabla V|\psi(t)\rangle e^{i\omega t} dt$, where ω is the emitted-proton frequency.

III. HHG MECHANISM OF POLAR MOLECULES IN ULTRASHORT PULSES

The harmonic spectra from HeH^{2+} for different CEPs ($\phi = 0, \pi/2, \pi, 3\pi/2$) are shown in Fig. 1. Here, we consider the parallel orientation with $\theta = 0^\circ$. For the case of $\phi = 0$ and π, as shown in Fig. 1(a), the harmonic spectra of these two CEPs have the same cutoff position near to the energy of $\omega = 19.7$ a.u. (corresponding to the electron kinetic energy of $E_p = \omega - I_p = 2.7U_p$ where $I_p = |E_0|$ is the ionization potential and $U_p = \varepsilon_0^2/(4\omega_0^2)$ is the ponderomotive energy). The spectrum for $\phi = 0$ (the solid-black curve) shows only one plateau, while the spectrum for $\phi = \pi$ (the dashed-red curve) exhibits two plateaus with the first cutoff at $\omega = 7.1$ a.u. (corresponding to $E_p = 0.75U_p$). It is noticeable that the yields of harmonics for $\phi = 0$ are several orders of magnitude higher than those for $\phi = \pi$ in the high-energy region. In Fig. 1(b), the first cutoff in the spectrum of $\phi = \pi/2$ (the solid-black curve) is located at $\omega = 3.6$ a.u. (corresponding to $E_p = 0.2U_p$) and it is located at $\omega = 13$ a.u. (corresponding to $E_p = 1.67U_p$) for the spectrum of $\phi = 3\pi/2$ (the dashed-red curve). Each of these two spectra in Fig. 1(b) ends with a high-energy cutoff at $\omega = 23.2$ a.u., which is higher than that of $\omega = 19.7$ a.u. in Fig. 1(a). These two spectra in Fig. 1(b) are of similar intensity below $\omega = 13$ a.u., then the spectrum for $\phi = 3\pi/2$ comes down, being nearly three orders of magnitude lower than that for $\phi = \pi/2$. These results show that the HHG spectra from HeH^{2+} in ultrashort laser pulses depend strongly on the CEP and present a multiplateau structure.

It should be stressed that this multiplateau structure is striking only for ultrashort laser pulses. For long pulses such as a nine-cycle pulse, this structure disappears and the difference between the spectra obtained with CEPs ϕ having a π phase difference also becomes negligible in our simulations. In addition, this structure does not depend strongly on the fundamental frequency used. For a three-cycle short pulse with the 400-nm laser wavelength or the 800-nm one, the spectra obtained with $\phi = \pi$ or $3\pi/2$ still show a remarkable multiplateau structure, similar to the cases of 600 nm shown in Fig. 1.

This multiplateau structure, characterized by the pronounced dips in the spectra for $\phi = \pi$ and $3\pi/2$, is closely associated with the mechanism of asymmetric ionization [37]. Specifically, the ionization of the asymmetric system in one laser cycle is weak as the laser polarization is parallel to the permanent dipole of the asymmetric system and strong for the antiparallel case. The dips are related to the parallel case. Next, we explore the potential mechanism in detail.

First, this CEP dependence of HHG spectra can be further understood through the Gabor analysis of the TDSE dipole acceleration [41–43] combined with the quantum-orbit theory (QOT) [44–46] (also see the Appendix). In Fig. 2, we plot the electron trajectories of the first return with the excursion time of the electron shorter than one optical cycle (the white-sphere curve), predicted from the QOT. The emission times of harmonics (i.e., the return times t_r of the recombination electrons) follow two typical electron trajectories labeled as $L1$ and $L2$ for the cases of $\phi = 0$ and π, as shown in Figs. 2(a) and 2(b). In contrast, when the CEP equals to $\pi/2$ or $3\pi/2$, there are three possible electron trajectories, labeled as $L3$, $L4$, and $L5$, contributing to the harmonic emission, as seen in Figs. 2(c) and 2(d).

The Gabor analysis results corresponding to the spectra in Fig. 1 are shown using the color coding in Fig. 2. One can observe that the Gabor-analysis results agree well with the predictions of QOT, with the distributions following the QOT trajectories with different amplitudes. The distribution for $\phi = 0$ and π in Figs. 2(a) and 2(b) implies two possible HHG cutoffs. The first one with $E_p = 2.7U_p$ appears around the return time $t_r = 1.93T$ and the second one with $E_p = 0.75U_p$ appears around $t_r = 2.4T$. These values are corresponding to the two HHG cutoffs in Fig. 1(a) located at $\omega = 19.7$ and

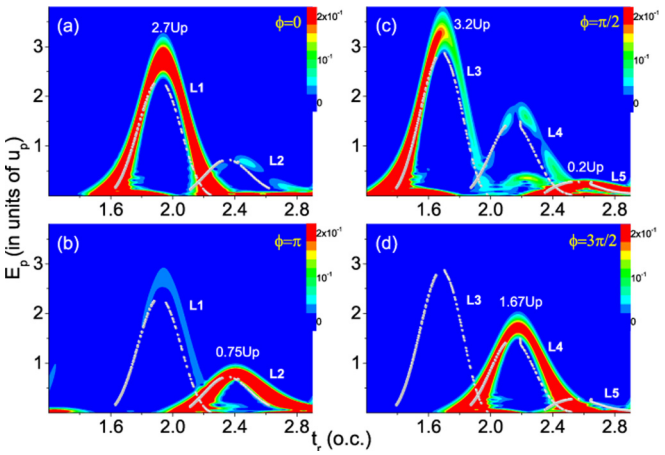

FIG. 2. Rescattering time and energy distribution of HHG (the color coding) from HeH^{2+} exposed to a three-cycle laser pulse for different CEPs of (a) $\phi = 0$, (b) π, (c) $\pi/2$, and (d) $3\pi/2$ at $\theta = 0^\circ$. In each panel, the white-sphere curve shows the electron trajectories for the first return, obtained from the QOT and labeled using the symbols of $L1$ to $L5$. The laser parameters are as in Fig. 1.

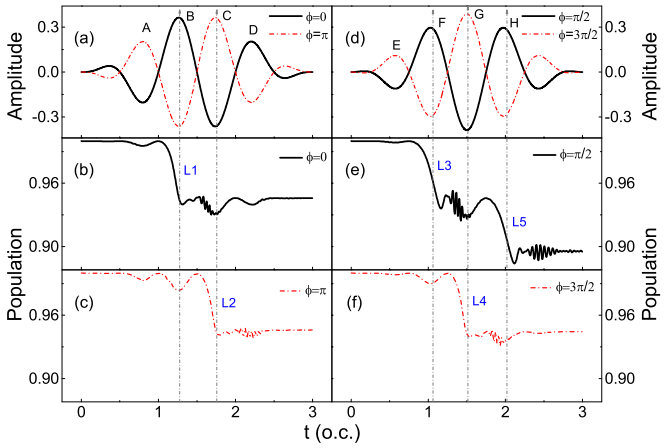

FIG. 3. The electric field of a three-cycle laser pulse with different CEPs of (a) $\phi = 0$ and π and (d) $\phi = \pi/2$ and $3\pi/2$, and the population of the ground state $|\langle 0|\psi(t)\rangle|^2$ of HeH^{2+} in this pulse for (b) $\phi = 0$, (c) $\phi = \pi$, (e) $\phi = \pi/2$, and (f) $\phi = 3\pi/2$ at $\theta = 0^\circ$. The laser parameters are as in Fig. 1. The positive peaks of the pulses with different CEPs are labeled using the characters of A-H. The vertical arrows are used to guide the eye. The blue symbols indicate the corresponding trajectories (introduced in Fig. 2) to which the strong ionization near a positive peak of the pulse can contribute.

7.1 a.u., respectively. Furthermore, in Fig. 2(a), the amplitude of the distribution along the trajectory $L2$ can be ignored compared to the $L1$ one. This is the reason why the spectrum for $\phi = 0$ shows only one plateau. In contrast, as shown in Fig. 2(b), the distribution along the trajectory $L2$ with a cutoff of $E_p = 0.75U_p$ has an amplitude much larger than that along $L1$ with the cutoff of $E_p = 2.7U_p$. Therefore, for the case of $\phi = \pi$, the harmonic intensity in the first plateau is much higher than that in the second one. The distributions in the right column of Fig. 2 indicate three cutoffs in the harmonic spectra with $E_p = 0.2U_p$, $1.67U_p$, and $3.2U_p$ (corresponding to the energy of $\omega = 3.6$, 13, and 23.2 a.u., respectively). For $\phi = \pi/2$ in Fig. 2(c), the distribution along the trajectory $L5$ peaked at $E_p = 0.2U_p$ has the largest amplitude, and the $L3$ one with a cutoff at $E_p = 3.2U_p$ has a comparable amplitude with the former one. For the case of $\phi = 3\pi/2$, the distribution along the trajectory $L4$ returning around $t_r = 2.2T$ has the largest amplitude, while the amplitude of $L3$ is rather weak. That is why the second plateau of 23 a.u. is much lower than the first one of 13 a.u. in the spectrum of $\phi = 3\pi/2$, as shown in Fig. 1(b). These results in Fig. 2 clearly show that both the amplitude and the return time of electron trajectories are sensitive to the CEP, which is the origin of the CEP dependence of the multiplateau structure in the HHG spectra.

The amplitude and emission time of HHG are closely related to the ionization process. In the following, we further analyze the ionization of the system. For a three-cycle laser pulse used here, a consequence of the ultrashort duration is the rapid variation of the laser intensity. As the ionization is closely associated with the depletion of the ground state in ultrashort pulses, we analyze the ionization of the system through the time-dependent population of the field-free ground state. Note, the "population" obtained by simply projecting onto the field-free ground state may not reflect the true dynamics of the system. Our extended simulations with the TDSE propagated in the eigenstate-energy representation [37,47] show that in ultrashort laser pulses the time-dependent ionization probability of the system evaluated with $1 - \langle 0|\psi(t)\rangle^2$ is comparable with the exact one obtained with $1 - \sum_n \langle n|\psi(t)\rangle^2$. Here $|0\rangle$ denotes the ground state and $|n\rangle$ denotes the bound state of the system. For simplicity, here, we neglect the influence of other bound states in our analyses. Similar analyses have also been performed in [35].

The time-dependent electric fields and the ground-state populations are presented in Fig. 3. The peaks of the pulses with different CEPs are labeled as A-H in Figs. 3(a) and 3(d). From the populations of the ground state in the second and the third rows of Fig. 3, one can see that the ionization (corresponding to the depletion of the ground state) mainly occurs in the central cycle of the pulse and also shows the obvious dependence on CEP. Specifically, in Fig. 3(b), as the CEP equals zero ($\phi = 0$), the ionization mainly occurs near to peak B of the laser field. By comparison, there are only a small amount of electrons to ionize near to peak C with negative maximum. The situation reverses in Fig. 3(c) for $\phi = \pi$, where the ionization probability increases sharply near to peak C. Similarly, in Figs. 3(e) and 3(f) with $\phi = \pi/2$ and $3\pi/2$, the ionization mainly occurs near to peaks F and H or peak G, respectively.

The phenomena revealed above can be understood by the inherent asymmetry of the HeH^{2+} molecule. The latter has a permanent dipole which is directing from the He nucleus to the H nucleus. It is well known that when the laser polarization is antiparallel (parallel) to the permanent dipole, the ground-state energy of the molecule is dressed up (down) and the ionization is enhanced (weakened) [34,35,37]. Due to this effect, in our cases, the ionization is stronger near the positive peaks of the field (at which the laser polarization is antiparallel to the permanent dipole) than that near the negative peaks of the field (the parallel case). Since the direction of the laser field in the

middle cycle of the pulse depends on the CEP, the ionization also does so.

Further analyses based on QOT show that the electron which ionizes near peak B will contribute to the trajectory $L1$ and that near C will contribute to $L2$. Similarly, the electron released near F will contribute to $L3$, that near G will contribute to $L4$, and that near H will contribute to $L5$. As a result, the main contributions to HHG for $\phi = 0$ come from the $L1$ trajectory with a large cutoff and those for $\phi = \pi$ come from the $L2$ trajectory with a small cutoff. Similarly, it is the $L3$ trajectory with a large cutoff for $\phi = \pi/2$ and the $L4$ one with the small one for $\phi = 3\pi/2$. These analyses explain the remarkable difference for the spectra with CEPs of ϕ_0 versus $\phi_0 + \pi$ in the high-energy region observed in each panel of Fig. 1.

IV. CALIBRATING THE DEGREE OF ORIENTATION WITH HHG

So far our discussions focus on the perfect orientation of the asymmetric molecule, which is impossible in real experiments. As the degree of orientation cannot be directly measured in experiments, the ratio of even versus odd HHG yields (even-odd ratio) has been used for calibrating the degree of orientation of the asymmetric system approximately [15,16]. To explore the influence of degree of orientation on HHG from asymmetric molecules in ultrashort pulses, as in [15], we assume that the molecules are perfectly aligned but only partially oriented, with n_u molecules pointing up (for which the permanent dipole is antiparallel to the x axis) and n_d pointing down (parallel). Here, we set n_u larger than n_d. Then the degree of orientation can be defined as $\langle \cos\theta \rangle = (n_u - n_d)/(n_u + n_d)$.

Due to the symmetry, the interchange of the positions of these two nuclei with the laser field having a CEP of $\phi = \phi_0$ is similar to the change of the CEP by $\phi = \phi_0$ to $\phi_0 + \pi$ with the positions of these nuclei unchanged. Specifically, in our simulations, the HHG power spectra obtained for molecules pointing up (down) correspond to those obtained for the cases of $\phi = 0$ or $\pi/2$ ($\phi = \pi$ or $3\pi/2$) in Fig. 1. To keep these points in mind, one can understand the spectra obtained with different degrees of orientation.

The HHG spectra of model HeH^{2+} for different degrees of orientation are plotted in Fig. 4. In each panel in Fig. 4, the difference between these two spectra in the high-energy region increases remarkably as the degree of orientation increases, implying that the degree of orientation has an important influence on this energy region. Specifically, for $\langle \cos\theta \rangle = 0.3$, the HHG yields in the high-energy region for $\phi = 0$ ($\phi = \pi/2$) are only several times higher than those for $\phi = \pi$ ($\phi = 3\pi/2$), as seen in Figs. 4(a) and 4(c). For $\langle \cos\theta \rangle = 0.6$ in Figs. 4(b) and 4(d), they differ by one order of magnitude. For the case of $\langle \cos\theta \rangle = 1$ in Figs. 1(a) and 1(b), there are several orders of magnitude of difference for these two spectra with different CEPs in the high-energy region.

By comparison, the low-energy region of the spectrum is not sensitive to the degree of orientation. In this region, these two spectra are similar in each panel in Fig. 4. As discussed before, the high-energy region of the spectrum in ultrashort pulses is sensitive to the CEP due to asymmetric ionization

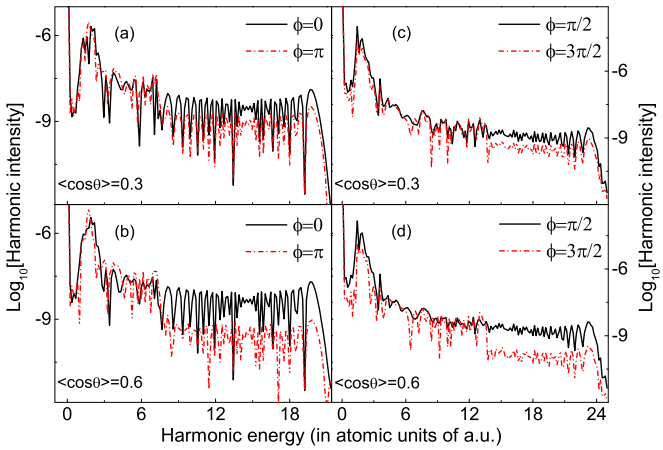

FIG. 4. Same as Fig. 1, but obtained with degrees of orientation of (a, c) $\langle \cos\theta \rangle = 0.3$ and (b, d) $\langle \cos\theta \rangle = 0.6$.

and therefore to the degree of orientation. Is it possible to use the spectrum in the high-energy region as a tool to probe the degree of orientation?

To answer this question, we first explore the relation between the degree of orientation and the HHG spectra of asymmetric molecules in ultrashort pulses. As discussed in [48], the coherent part of the HHG spectrum parallel to the laser polarization for perfect orientation can be approximately as $F(\omega,\theta) \approx \int d\mathbf{p}[a(\mathbf{p},\theta)\langle 0|\vec{\mathbf{e}}\cdot\nabla V|\mathbf{p}\rangle]$. Here, $a(\mathbf{p},\theta) = \int dt[a_0^*(t)c_\mathbf{p}(t)e^{i\omega t}]$ is the spectral amplitude. $a_0(t) = \langle 0|\psi(t)\rangle$ and $c_\mathbf{p}(t) = \langle p|\psi(t)\rangle$. $\vec{\mathbf{e}}$ is the unit vector along the laser polarization. $V \equiv V(\mathbf{r})$ is the Coulomb potential as defined in Sec. II. $\langle 0|\nabla V|\mathbf{p}\rangle$ is the dipole acceleration between the continuum state $|\mathbf{p}\rangle$ and the ground state $|0\rangle$. $|\psi(t)\rangle$ is the time-dependent wave function. Assuming that the main contribution to the harmonic ω comes from the electron with energy $E_p = \mathbf{P}^2/2$ agreeing with the energy conservation relation $\omega = E_p + I_p$, we have $F(\omega,\theta) \approx a(\mathbf{p},\theta)\langle 0|\vec{\mathbf{e}}\cdot\nabla V|\mathbf{p}\rangle$ [3]. Here, I_p is the ionization potential of the system. The spectral amplitude $a(\mathbf{p},\theta)$ is closely related to the amplitude $c_\mathbf{p}(t)$ of the continuum electron, which can be expected to be larger for stronger ionization of the system.

If we assume that the degree of orientation is $\langle \cos\theta \rangle = M$, and the total numbers of molecules pointing up and down are $M_T = M_u + M_d$, we have $M_u = (1+M)M_T/2$ and $M_d = (1-M)M_T/2$. The coherent part of the HHG spectrum F_M with the degree of orientation M can be written as

$$F_M(\omega,\theta) = [M_u a_u(\mathbf{p},\theta) + M_d a_d(\mathbf{p},\theta)]\langle 0|\vec{\mathbf{e}}\cdot\nabla V|\mathbf{p}\rangle. \quad (1)$$

Here, $a_{u(d)}$ is the spectral amplitude for the case of molecules pointing up (down) with perfect orientation. As discussed above, for the ultrashort laser pulse, due to the permanent-dipole effect, the main contribution to HHG in the high-energy region comes from the molecules pointing up (for which the permanent dipole is antiparallel to the x axis), so we have $|a_u(\mathbf{p},\theta)| \gg |a_d(\mathbf{p},\theta)|$. Therefore, the HHG spectrum F_M^h in the high-energy region can be approximately as

$$F_M^h(\omega,\theta) \approx M_u a_u(\mathbf{p},\theta)\langle 0|\vec{\mathbf{e}}\cdot\nabla V|\mathbf{p}\rangle. \quad (2)$$

The power spectrum is $S_M^h(\omega,\theta) = |F_M^h(\omega,\theta)|^2 = M_u^2|a_u(\mathbf{p},\theta)|^2|\langle 0|\vec{\mathbf{e}}\cdot\nabla V|\mathbf{p}\rangle|^2$. The integrated HHG yield

T_M^h in the high-energy region can be written as

$$T_M^h(\theta) \approx \int_\Omega d\omega S_M^h(\omega,\theta) = M_u^2 P_u(\theta), \quad (3)$$

where Ω is the integral domain which is located in the second plateau of the spectra as seen in Fig. 4, and $P_u(\theta) = \int_\Omega d\omega |a_u(\mathbf{p},\theta)|^2 |\langle 0|\vec{\mathbf{e}}\cdot\nabla V|\mathbf{p}\rangle|^2$. The ratio of harmonic yields in this region for $\langle\cos\theta\rangle = M$ versus $\langle\cos\theta\rangle = 0$ (random orientation with $M_u = M_d = M_0$) is given by

$$\frac{T_M^h(\theta)}{T_0^h(\theta)} = \frac{M_u^2}{M_0^2} = (1+M)^2. \quad (4)$$

The above expression predicts that this ratio is insensitive to the laser parameters. Note, Eq. (4) is applicable only for polar molecules with a large permanent dipole for which the asymmetric ionization plays an important role in HHG. For molecules with a small permanent dipole such that the amplitude $a_u(\mathbf{p},\theta)$ is comparable with $a_d(\mathbf{p},\theta)$ in Eq. (1), the amplitude $a_d(\mathbf{p},\theta)$ cannot be omitted and the expressions of Eqs. (2) and (4) are not applicable. Assuming that $a_u(\mathbf{p},\theta)$ and $a_d(\mathbf{p},\theta)$ are not sensitive to the momentum $\mathbf{p}$, we have $a_u(\mathbf{p},\theta) \approx a_u(\theta) \equiv a$ and $a_d(\mathbf{p},\theta) \approx a_d(\theta) \equiv b$. In this case, we have

$$\frac{T_M^h(\theta)}{T_0^h(\theta)} = \frac{|aM_u + bM_d|^2}{|aM_0 + bM_0|^2} = \frac{|(a+b)+(a-b)M|^2}{|a+b|^2}. \quad (5)$$

This above expression shows that in the extreme cases of nondipole molecules with $a = b$, the ratio should always be 1. In addition, For $M = 0$, this ratio should also be 1. In particular, the interference between the two amplitudes $a \equiv a_u(\mathbf{p},\theta)$ and $b \equiv a_d(\mathbf{p},\theta)$ can also play an important role in this ratio. For example, for $M = 1$, we have $\frac{T_M^h(\theta)}{T_0^h(\theta)} = \frac{4|a|^2}{|a+b|^2}$. This ratio can be smaller than 4 when a constructive interference occurs (i.e., $|a+b| > |a|$). It can be larger than 4 for the destructive one with $|a+b| < |a|$. Below, we will focus on the relation of Eq. (4) for polar molecules with a large permanent dipole.

In Fig. 5, we plot this ratio obtained with the analytical expression of $(1+M)^2$ using the dark-cyan spheres. It increases as the degree of orientation increases. Here, we also present this ratio obtained with the TDSE evaluations of $T_M^h(\theta)/T_0^h(\theta)$ for different laser parameters. The integrals in $T_M^h(\theta)$ and $T_0^h(\theta)$ are performed around the cutoff region of the second plateau. For the case of $\phi = 0$ with $\theta = 0^\circ$ in Fig. 5(a), the TDSE results with different laser parameters agree well with the analytical one. For the case of $\phi = \pi/2$, the agreement holds except for a slight deviation for the case of $I = 4\times10^{15}$ W/cm^2, as seen in Fig. 5(c). Our further simulations show that even for the case of $\theta = 30^\circ$, the TDSE results for this ratio with different laser intensities and CEPs are similar to the analytical one of $(1+M)^2$, as shown in Figs. 5(b) and 5(d). As we change the driving laser wavelength, a good agreement between the TDSE and the analytical results is also observed, as shown in Fig. 6. The above results show that this ratio of $T_M^h(\theta)/T_0^h(\theta)$ provides a potential way for evaluating the degree of orientation of the asymmetric system.

To check our results, we also simulate the HHG from HeH^{2+} with $R = 2$ a.u.. These results are presented in Fig. 7(a). One can observe that the TDSE evaluation of $T_M^h(\theta)/T_0^h(\theta)$ also gives an applicable prediction of the degree of orientation. It is

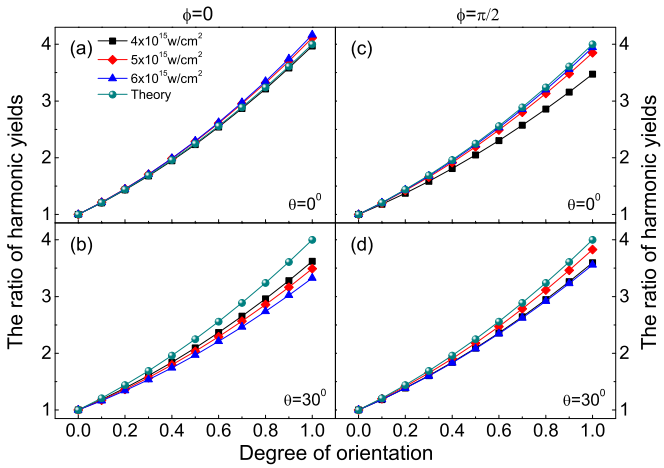

FIG. 5. The ratio of harmonic yields of HeH^{2+} in the high-energy region for $\langle\cos\theta\rangle = M$ vs $\langle\cos\theta\rangle = 0$ (random orientation), obtained with different laser intensities and calculated by different methods. The left (right) column shows the results for CEP $\phi = 0$ ($\phi = \pi/2$). The laser intensities and the orientation angles θ are as shown. The laser wavelength is $\lambda = 600$ nm. The analytical results of $(1+M)^2$ are plotted using the dark-cyan spheres and other curves show the TDSE results of $T_M^h(\theta)/T_0^h(\theta)$. See the context for more details.

well known that the HeH^{2+} molecule has a stable 2σ excited state. In Fig. 7(b), we also show the results obtained for HeH^{2+} with $R = 4$ a.u. initially in the 2σ state (the first excited state of HeH^{2+}). A good agreement between the TDSE results of $T_M^h(\theta)/T_0^h(\theta)$ and the analytical one of $(1+M)^2$) can also observed here.

Finally, we also performed calculations for polar molecules with more complex asymmetries such as BF and CO with 5σ symmetry [49]. To simulate the HHG from these molecules,

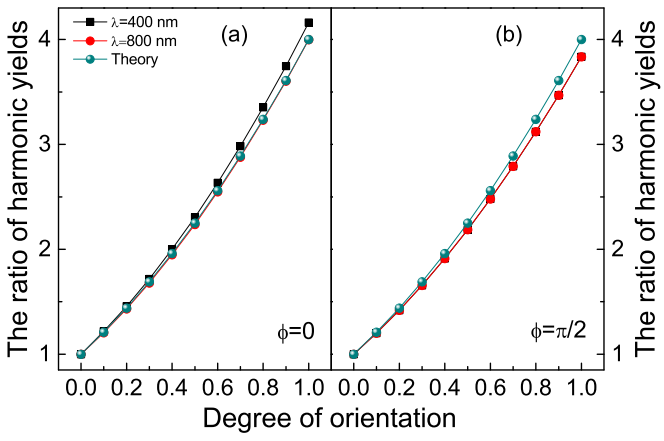

FIG. 6. The ratio of harmonic yields of HeH^{2+} in the high-energy region for $\langle\cos\theta\rangle = M$ vs $\langle\cos\theta\rangle = 0$ (random orientation), at $\phi = 0$ (a) and $\phi = \pi/2$ (b), obtained with different laser wavelengthes and calculated by different methods. The laser intensity is $I = 5\times10^{15}$ W/cm^2. The analytical results of $(1+M)^2$ are plotted using the dark-cyan spheres and other curves show the TDSE results of $T_M^h(\theta)/T_0^h(\theta)$.

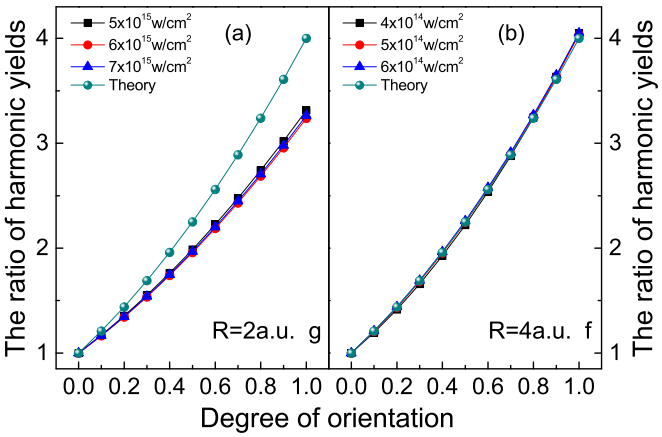

FIG. 7. The ratio of harmonic yields in the high-energy region for $\langle\cos\theta\rangle = M$ vs $\langle\cos\theta\rangle = 0$ (random orientation), obtained with different laser intensities and calculated by different methods. In (a), we show the results for HeH^{2+} with $R = 2$ a.u. initially in the ground state as in Fig. 5 (denoted using the character "g"). In (b), we show the results for HeH^{2+} with $R = 4$ a.u. initially in the first excited state (denoted using the character "f"). The CEP used here is $\phi = 0$ and the orientation angle is $\theta = 0^\circ$. The laser intensities are as shown. The laser wavelengthes are $\lambda = 600$ nm in (a) and $\lambda = 800$ nm in (b). The analytical results of $(1 + M)^2$ are plotted using the dark-cyan spheres and other curves show the TDSE results of $T_M^h(\theta)/T_0^h(\theta)$.

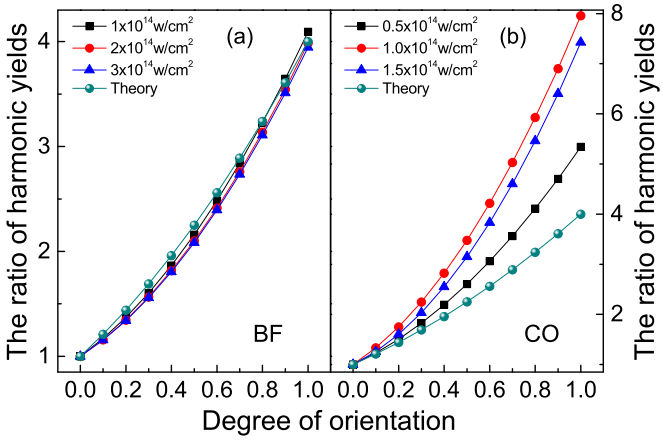

FIG. 8. The ratio of harmonic yields in the high-energy region for $\langle\cos\theta\rangle = M$ vs $\langle\cos\theta\rangle = 0$ (random orientation), obtained with different laser intensities and calculated by different methods. In (a), we show the results for BF. In (b), we show the results for CO. The CEP used here is $\phi = 0$ and the orientation angle is $\theta = 0^\circ$. The laser intensities are as shown. The laser wavelength is $\lambda = 1400$ nm in each panel. The analytical results of $(1 + M)^2$ are plotted using the dark-cyan spheres and other curves show the TDSE results of $T_M^h(\theta)/T_0^h(\theta)$.

we use the model potential similar to that used in [12]. That is,

$$V(\mathbf{r}) = -\sum_{j=1,2} \frac{(Z_{ji} - Z_{jo})\exp\left(-\rho\mathbf{r}_j^2\right) + Z_{jo}}{\sqrt{\xi + \mathbf{r}_j^2}}, \qquad (6)$$

where Z_1 and Z_2 are the screened effective nuclear charges for the O center and the C center (or the F center and the B center), respectively. The indices i and o denote the inner and outer limits of Z_1 and Z_2. ξ and ρ are the softening and the screening parameters with $\xi > 0$ and $\rho > 0$. $\mathbf{r}_j = \mathbf{r} - \mathbf{R}_j$ with $\mathbf{R}_1$ and $\mathbf{R}_2$ being the positions of the nuclei that have the coordinates (x_1, y_1) and (x_2, y_2) in the xoy plane. $x_{1/2} = \pm R_{1/2}\cos\theta$, $y_{1/2} = \pm R_{1/2}\sin\theta$, $R_1 = R/(1 + \beta)$, $R_2 = \beta R/(1 + \beta)$ with $\beta = Z_1/Z_2$. R is the internuclear separation. Here, we use the parameters of $Z_{1i} = 6, Z_{2i} = 4, Z_{1o} = 0.6$, $Z_{2o} = 0.4$ with $\beta = Z_{1i}/Z_{2i} = Z_{1o}/Z_{2o}$, $R = 2.13$ a.u., $\xi = 0.5$, and $\rho = 1.746$ for CO. For BF, these relevant parameters are $Z_{1i} = 7, Z_{2i} = 3, Z_{1o} = 0.7$, $Z_{2o} = 0.3$ with $\beta = Z_{1i}/Z_{2i} = Z_{1o}/Z_{2o}$, $R = 2.385$ a.u., $\xi = 0.5$, and $\rho = 2.27$. With these parameters, the ionization potentials of HOMO reproduced here are $I_p = 0.51$ a.u. for CO and $I_p = 0.41$ a.u. for BF. Note, in comparison with BF, the CO molecule has a smaller permanent dipole here. Relevant results are presented in Fig. 8.

One can observe that as the TDSE results agree well with the analytical one for BF in Fig. 8(a), they differ remarkably from the analytical one for CO in Fig. 8(b). As introduced above, the expression of Eq. (4) is applicable only for asymmetric molecules with a large permanent dipole (i.e., the asymmetry of the molecular orbital is strong or the value of $\langle 0|\mathbf{r}|0\rangle$ evaluated is large). For asymmetric molecules with a small one (i.e., this asymmetry is weak or the value of $\langle 0|\mathbf{r}|0\rangle$ is small), the ionization yields do not differ remarkably for these two cases where the laser polarization is parallel or antiparallel to the permanent dipole. So the approximation in Eq. (2) cannot be performed and Eq. (4) is not applicable.

For the case of CO with weak asymmetry, one can also observe from Fig. 8 that the TDSE ratio of $T_M^h(\theta)/T_0^h(\theta)$ is larger than theoretical values. As discussed below Eq. (5), a destructive interference between these two amplitudes of $a \equiv a_u(\mathbf{p},\theta)$ and $b \equiv a_d(\mathbf{p},\theta)$ for molecules pointing up and down can occur here. It should also be stressed that although this ratio of $T_M^h(\theta)/T_0^h(\theta)$ is not sensitive to the laser parameters, in real experiments, relatively low laser intensities with relatively long laser wavelengthes are preferred at which macroscopic phase mismatch of HHG is weak [29,50,51].

V. CONCLUSION

In summary, we have studied the HHG from oriented asymmetric molecules in ultrashort laser pulses considering imperfect orientation. The HHG spectra obtained show a striking multiplateau structure which depends strongly on the degree of orientation of the asymmetric system. We identify the important role of the permanent-dipole effect in shaping the structure. When this effect is sensitive to the degree of orientation, the multiplateau structure does so. Based on these results, an alternative procedure, which is not strongly dependent on the CEP and the laser intensity, is proposed to probe the degree of orientation using the HHG in ultrashort laser pulses. Our paper gives suggestions on experiments involving the orientation of the asymmetric system.

ACKNOWLEDGMENTS

This work was supported by the National Basic Research Program of China (Grant No. 2013CB328702), the National Natural Science Foundation of China (Grants No. 11274090, No. 11374074, and No. 11504069), the Fundamental Research

Funds for the Central Universities (Grant No. GK201403002), and Natural Science Foundation of Hebei province (Grant No. A2015205161).

APPENDIX: QUANTUM ORBITS

The QOT arises from the well-known strong-field approximation (SFA) for HHG [44–46]. According to the SFA, the intensity of the Nth harmonic is defined as the Fourier component of the time-dependent dipole

$$F_N = i\int_0^T dt e^{iN\omega_0 t}\int_0^t dt'\int d^3\mathbf{p}D(\mathbf{p},t,t')e^{-iS}, \quad \text{(A1)}$$

with the product of dipole matrix elements

$$D(\mathbf{p},t,t') = \langle\psi_0|\mathbf{r}|\mathbf{p}+\mathbf{A}(t)\rangle\langle\mathbf{p}+\mathbf{A}(t')|\mathbf{r}|\psi_0\rangle E(t'), \quad \text{(A2)}$$

and the quasiclassical action

$$S \equiv S(\mathbf{p},t,t') = \int_{t'}^t dt''\{[\mathbf{p}+\mathbf{A}(t'')]^2/2 + I_p\}, \quad \text{(A3)}$$

where $\mathbf{p}$ is the canonical momentum, $\mathbf{A}(t) = -\int^t \mathbf{E}(t')dt'$ is the vector potential of the laser field $\mathbf{E}(t)$, $|\psi_0\rangle$ is the ground state of the system, and $|\mathbf{p}\rangle$ is the plane wave. Because the quasiclassical action varies much faster than the other factors in Eq. (A1), the integral over the momentum in Eq. (A1) can be performed using the saddle-point method, with the following conditions [44,52,53]:

$$[\mathbf{p}_{st}(t_\mathrm{i},t_\mathrm{r}) + \mathbf{A}(t_\mathrm{i})]^2/2 = -I_p, \quad \text{(A4)}$$

$$[\mathbf{p}_{st}(t_\mathrm{i},t_\mathrm{r}) + \mathbf{A}(t_\mathrm{r})]^2/2 = N\omega_0 - I_p. \quad \text{(A5)}$$

Here, we have used the symbols of $t_i \equiv t'$ and $t_r \equiv t$. $\mathbf{p}_{st}(t_\mathrm{i},t_\mathrm{r}) = -\int_{t_\mathrm{i}}^{t_\mathrm{r}} \mathbf{A}(t'')dt''/(t_\mathrm{r}-t_\mathrm{i})$ is the saddle-point electron momentum.

For $I_p \neq 0$, the solutions of Eqs. (A4) and (A5) for t_i and t_r are complex and have been termed as quantum orbits. The real parts of t_i and t_r are interpreted as the physical ionization time and the return time of the rescattering electron (the return time t_r is also considered as the emission time of the Nth harmonic), and the imaginary part of t_i can be interpreted as a tunneling time [44]. In our simulations, these two complex equations of Eqs. (A4) and (A5) are solved numerically using the Newton-Raphson method.

It should be noted that Eqs. (A4) and (A5) are applicable for atoms. For molecules, it has been shown that the internuclear distance R also needs to be considered in QOT, especially for molecules with large R [54,55]. For the present cases with R smaller than 4 a.u. explored in the paper, our extended simulations show that the influence of the internuclear distance on quantum orbits of the molecular system is small. So we neglect the influence of the internuclear distance in our discussions.

[1] H. Stapelfeldt and T. Seideman, *Colloquium:* Aligning molecules with strong laser pulses, Rev. Mod. Phys. **75**, 543 (2003).

[2] F. Krausz and M. Ivanov, Attosecond Physics, Rev. Mod. Phys. **81**, 163 (2009).

[3] J. Itatani, J. Levesque, D. Zeidler, Hiromichi Niikura, H. Pepin, J. C. Kieffer, P. B. Corkum, and D. M. Villeneuve, Tomographic imaging of molecular orbitals, Nature (London) **432**, 867 (2004).

[4] O. Smirnova, Y. Mairesse, S. Patchkovskii, N. Dudovich, D. Villeneuve, P. Corkum and M. Yu. Ivanov, High harmonic interferometry of multi-electron dynamics in molecules, Nature (London) **460**, 972 (2009).

[5] H. J. Wörner, J. B. Bertrand, D. V. Kartashov, P. B. Corkum, and D. M. Villeneuve, Following a chemical reaction using high-harmonic interferometry, Nature (London) **466**, 604 (2010).

[6] H. Sakai, S. Minemoto, H. Nanjo, H. Tanji, and T. Suzuki, Controlling the Orientation of Polar Molecules with Combined Electrostatic and Pulsed, Nonresonant Laser Fields, Phys. Rev. Lett. **90**, 083001 (2003).

[7] J. L. Hansen, L. Holmegaard, L. Kalhøj, S. L. Kragh, H. Stapelfeldt, F. Filsinger, G. Meijer, J. Küpper, D. Dimitrovski, M. Abu-samha, C. P. J. Martiny, and L. B. Madsen, Ionization of one- and three-dimensionally-oriented asymmetric-top molecules by intense circularly polarized femtosecond laser pulses, Phys. Rev. A **83**, 023406 (2011).

[8] S. Fleischer, Y. Zhou, R. W. Field, and K. A. Nelson, Molecular Orientation and Alignment by Intense Single-Cycle THz Pulses, Phys. Rev. Lett. **107**, 163603 (2011).

[9] M. Spanner, S. Patchkovskii, E. Frumker, and P. Corkum, Mechanisms of Two-Color Laser-Induced Field-Free Molecular Orientation, Phys. Rev. Lett. **109**, 113001 (2012).

[10] P. Babilotte, K. Hamraoui, F. Billard, E. Hertz, B. Lavorel, O. Faucher, and D. Sugny, Observation of the field-free orientation of a symmetric-top molecule by terahertz laser pulses at high temperature, Phys. Rev. A **94**, 043403 (2016).

[11] Y. J. Chen and B. Zhang, Tracing the structure of asymmetric molecules from high-order harmonic generation, Phys. Rev. A **84**, 053402 (2011).

[12] Y. J. Chen, L. B. Fu, and J. Liu, Asymmetric Molecular Imaging through Decoding Odd-Even High-Order Harmonics, Phys. Rev. Lett. **111**, 073902 (2013).

[13] P. M. Kraus, O. I. Tolstikhin, D. Baykusheva, A. Rupenyan, J. Schneider, C. Z. Bisgaard, T. Morishita, F. Jensen, L. B. Madsen, and H. J. Wörner, Observation of laser-induced electronic structure in oriented polyatomic molecules, Nat. Commun. **6**, 7039 (2015).

[14] W. Y. Li, S. J. Yu, S. Wang, and Y. J. Chen, Probing nuclear dynamics of oriented HeH+ with odd-even high-order harmonics, Phys. Rev. A **94**, 053407 (2016).

[15] E. Frumker, N. Kajumba, J. B. Bertrand, H. J. Wörner, C. T. Hebeisen, P. Hockett, M. Spanner, S. Patchkovskii, G. G. Paulus, D. M. Villeneuve, A. Naumov, and P. B. Corkum, Probing Polar Molecules with High Harmonic Spectroscopy, Phys. Rev. Lett. **109**, 233904 (2012).

[16] P. M. Kraus, A. Rupenyan, and H. J. Wörner, High-Harmonic Spectroscopy of Oriented OCS Molecules: Emission of Even and Odd Harmonics, Phys. Rev. Lett. **109**, 233903 (2012).

[17] P. M. Kraus, D. Baykusheva, and H. J. Wörner, Two-pulse orientation dynamics and high-harmonic spectroscopy of strongly-oriented molecules, J. Phys. B **47**, 124030 (2014).

[18] P. M. Kraus, D. Baykusheva, and H. J. Wörner, Two-Pulse Field-Free Orientation Reveals Anisotropy of Molecular Shape Resonance, Phys. Rev. Lett. **113**, 023001 (2014).

[19] P. M. Kraus, B. Mignolet, D. Baykusheva, A. Rupenyan, L. Horny, E. F. Penka, G. Grassi, O. I. Tolstikhin, J. Schneider, F. Jensen, L. B. Madsen, A. D. Bandrauk, F. Remacle, and H. J. Wörner, Measurement and laser control of attosecond charge migration in ionized iodoacetylene, Science **350**, 790 (2015).

[20] E. Frumker, C. T. Hebeisen, N. Kajumba, J. B. Bertrand, H. J. Wörner, M. Spanner, D. M. Villeneuve, A. Naumov, and P. B. Corkum, Oriented Rotational Wave-Packet Dynamics Studies via High Harmonic Generation, Phys. Rev. Lett. **109**, 113901 (2012).

[21] I. P. Christov, M. M. Murnane, and H. C. Kapteyn, High-Harmonic Generation of Attosecond Pulses in the "Single-Cycle" Regime, Phys. Rev. Lett. **78**, 1251 (1997).

[22] M. Schnürer, C. Spielmann, P. Wobrauschek, C. Streli, N. H. Burnett, C. Kan, K. Ferencz, R. Koppitsch, Z. Cheng, T. Brabec, and F. Krausz, Coherent 0.5-kev X-Ray Emission from Helium Driven by a Sub-10-fs Laser, Phys. Rev. Lett. **80**, 3236 (1998).

[23] T. Brabec and F. Krausz, Intense few-cycle laser fields: Frontiers of nonlinear optics, Rev. Mod. Phys. **72**, 545 (2000).

[24] P. B. Corkum and F. Krausz, Attosecond science, Nat. Phys. **3**, 381 (2007).

[25] O. Raz, O. Pedatzur, B. D. Bruner, and N. Dudovich, Spectral caustics in attosecond science, Nat. Photonics **6**, 170 (2012).

[26] P. B. Corkum, Plasma Perspective on Strong Field Multiphoton Ionization, Phys. Rev. Lett. **71**, 1994 (1993).

[27] A. de Bohan, P. Antoine, D. B. Milošević, and B. Piraux, Phase-Dependent Harmonic Emission with Ultrashort Laser Pulses, Phys. Rev. Lett. **81**, 1837 (1998).

[28] Y. Xiang, J. Lu, Y. Niu, and S. Gong, Measuring the carrier-envelope phases of few-cycle laser pulses using the high-order harmonic spectrum from asymmetric molecules, J. Phys. B **48**, 135601 (2015).

[29] Y. Z. Shi, S. Wang, F. L. Dong, Y. P. Li, and Y. J. Chen, Classical effect for enhanced high harmonic yield in ultrashort laser pulses with a moderate laser intensity, J. Phys. B **50**, 065004 (2017).

[30] S. Ben, T. Wang, T. T. Xu, J. Guo, and X. S. Liu, Nonsequential double ionization channels control of Ar with few-cycle elliptically polarized laser pulse by carrier-envelope-phase, Opt. Express **24**, 7525 (2016).

[31] A. Etches and L. B. Madsen, Extending the strong-field approximation of high-order harmonic generation to polar molecules: Gating mechanisms and extension of the harmonic cutoff, J. Phys. B **43**, 155602 (2010).

[32] W. Hong, Q. Zhang, X. Zhu, and P. Lu, Isolated attosecond pulse generation with the stability against the carrier-envelope phase shift and with the high-beam quality from CO gas medium, Opt. Express **19**, 26174 (2011).

[33] H. Du, L. Luo, X. Wang, and B. Hu, Generating isolated elliptically polarized attosecond pulses from oriented CO gas medium using linearly polarized driving pulses, Phys. Rev. A **86**, 013846 (2012).

[34] X. B. Bian and A. D. Bandrauk, Multichannel Molecular High-Order Harmonic Generation from Asymmetric Diatomic Molecules, Phys. Rev. Lett. **105**, 093903 (2010).

[35] Y. J. Chen and B. Zhang, Role of excited states in the emission times of harmonics from asymmetric molecules, Phys. Rev. A **86**, 023415 (2012).

[36] X. Y. Miao and H. N. Du, Theoretical study of high-order-harmonic generation from asymmetric diatomic molecules, Phys. Rev. A **87**, 053403 (2013).

[37] G. L. Kamta and A. D. Bandrauk, Phase Dependence of Enhanced Ionization in Asymmetric Molecules, Phys. Rev. Lett. **94**, 203003 (2005).

[38] G. L. Kamta, A. D. Bandrauk, and P. B. Corkum, Asymmetry in the harmonic generation from nonsymmetric molecules, J. Phys. B **38**, L339 (2005).

[39] M. D. Feit, J. A. Fleck Jr., and A. Steiger, Solution of the Schrödinger equation by a spectral method, J. Comput. Phys. **47**, 412 (1982).

[40] M. Lein, N. Hay, R. Velotta, J. P. Marangos, and P. L. Knight, Role of the Intramolecular Phase in High-Harmonic Generation, Phys. Rev. Lett. **88**, 183903 (2002).

[41] X.-M. Tong and S.-I. Chu, Probing the spectral and temporal structures of high-order harmonic generation in intense laser pulses, Phys. Rev. A **61**, 021802(R) (2000).

[42] J. J. Carrera, X. M. Tong, and S.-I. Chu, Creation and control of a single coherent attosecond xuv pulse by few-cycle intense laser pulses, Phys. Rev. A **74**, 023404 (2006).

[43] C. C. Chirilă, I. Dreissigacker, E. V. Van der Zwan, and M. Lein, Emission times in high-order harmonic generation, Phys. Rev. A **81**, 033412 (2010).

[44] M. Lewenstein, Ph. Balcou, M. Yu. Ivanov, A. L'Huillier, and P. B. Corkum, Theory of high-harmonic generation by low-frequency laser fields, Phys. Rev. A **49**, 2117 (1994).

[45] P. Salieres, B. Carre, L. Le Deroff, F. Grasbon, G. G. Paulus, H. Walther, R. Kopold, W. Becker, D. B. Milosevic, A. Sanpera, and M. Lewenstein, Feynman's path-integral approach for intense-laser-atom interactions, Science **292**, 902 (2001).

[46] D. B. Milošević and W. Becker, Role of long quantum orbits in high-order harmonic generation, Phys. Rev. A **66**, 063417 (2002).

[47] Y. Chen, Dynamic of rescattering-electron wave packets in strong and short-wavelength laser fields: Roles of Coulomb potential and excited states, Phys. Rev. A **84**, 043423 (2011).

[48] Y. J. Chen, J. Liu, and B. Hu, Intensity dependence of intramolecular interference from a full quantum analysis of high-order harmonic generation, Phys. Rev. A **79**, 033405 (2009).

[49] J. Heslar, D. Telnov, and S.-I. Chu, High-order-harmonic generation in homonuclear and heteronuclear diatomic molecules: Exploration of multiple orbital contributions, Phys. Rev. A **83**, 043414 (2011).

[50] V. S. Yakovlev, M. Ivanov, and F. Krausz, Enhanced phase-matching for generation of soft X-ray harmonics and attosecond pulses in atomic gases, Opt. Express **15**, 15351 (2007).

[51] M.-C. Chen, P. Arpin, T. Popmintchev, M. Gerrity, B. Zhang, M. Seaberg, D. Popmintchev, M. M. Murnane, and H. C. Kapteyn, Bright, Coherent, Ultrafast Soft X-Ray Harmonics Spanning the Water Window from a Tabletop Light Source, Phys. Rev. Lett. **105**, 173901 (2010).

[52] C. F. de Morisson Faria, D. B. Milošević, and G. G. Paulus, Phase-dependent effects in bichromatic high-order harmonic generation, Phys. Rev. A **61**, 063415 (2000).

[53] M. Lewenstein, P. Salières, and A. L'Huillier, Phase of the atomic polarization in high-order harmonic generation, Phys. Rev. A **52**, 4747 (1995).

[54] R. Kopold, W. Becker, and M. Kleber, Model calculations of high-harmonic generation in molecular ions, Phys. Rev. A **58**, 4022 (1998).

[55] J. Chen, S.-I. Chu, and J. Liu, Time-frequency analysis of molecular high-harmonic generation spectrum by means of wavelet transform and Wigner distribution techniques, J. Phys. B **39**, 4747 (2006).